IEEE Access
Multidisciplinary | Rapid Review | Open Access Journal

Received August 9, 2021, accepted August 29, 2021, date of publication August 30, 2021, date of current version September 10, 2021.

Digital Object Identifier 10.1109/ACCESS.2021.3109092

An Improved Pulse Voltage Injection Based Initial Rotor Position Estimation Method for PMSM

XIANG WU, (Member, IEEE), ZEHAO LV, ZANG LING, XIAO ZHANG, AND GUOJUN TAN, (Member, IEEE)
School of Electrical and Power Engineering, China University of Mining and Technology, Xuzhou 221008, China

Corresponding author: Guojun Tan (gjtan_cumt@163.com)

This work was supported in part by the Fundamental Research Funds for the Central Universities under Grant 2020QN64, and in part by the National Natural Science Foundation of China under Grant 52007190.

ABSTRACT It's essential to obtain the initial rotor position of PMSM to prevent the reversal of the rotor and to ensure the maximum electromagnetic torque output during the startup process. An improved pulse-voltage injection-based initial rotor position estimation method is proposed in this paper. Different from the conventional pulse-voltage-injection-based method that only utilizes the information about the virtual d-axis current for the voltage vector injected to PMSMs, the information about the virtual q-axis current is also utilized in the proposed method to reduce the estimation errors caused by the current sampling errors. The experimental results indicate that the estimation accuracy can be greatly improved.

INDEX TERMS Initial rotor position, permanent magnet synchronous machine (PMSM), pulse voltage injection.

I. INTRODUCTION

In applications of the position sensorless control for permanent-magnet synchronous motors (PMSMs) [1]–[4], the initial rotor position estimation method (IRPEM) is essential both to prevent the reversal of the rotor and to ensure the maximum electromagnetic torque output during the startup. The existing IRPEMs can be divided into two categories, i.e., high-frequency signals injection (HFSI) [5]–[12] and pulse signals injection (PSI) based methods [13]–[16].

For HFSI based methods, high-frequency sinusoidal [5]–[6] or square-wave signals [7]–[12] are injected to PMSMs and signal demodulation strategies are designed to estimate the initial rotor position (IRP) according to the high-frequency response of PMSMs. For the HFSI methods where high-frequency sinusoidal signals are injected, low-pass or (and) band-pass filters are usually adopted in the signal demodulation processes, which may cause long convergence time and limited control bandwidth. In [6], a direct signal demodulation method without low-pass and band-pass filters is proposed to improve the system stability and dynamic property. The HFSI based methods with square-wave injection have demonstrated advantages in the dynamic property and control bandwidth [7]–[9]. For the above HFSI methods, the polarity of the rotor magnet cannot be determined by the high-frequency response of PMSMs owing to the fact that the inductances of PMSMs vary periodically as a second spatial harmonics. Thus, extra magnetic polarity detection schemes are demanded [11], [12], which increases the complexity.

The PSI based methods estimate the IRP according to the current response model of PMSM in the case where the pulse voltages or currents are injected into different directions of motor windings, which can be divided into 2 types, i.e, the pulse voltage injection (PVI) and the pulse current injection (PCI). The methods proposed in [13], [14] are based on the principle that the virtual d-axis current for the voltage vector (VV) applied to PMSMs increases as the injected VV approaches to the north pole of the rotor. For the PSI based methods, the estimation accuracy is dependent on the amplitude of the injected VV, and the decision method of the optimal amplitude is studied in [13]. It is pointed out that the estimation accuracy is affected by the current sampling errors [15], and a novel procedure which combines an iteration of the pulses sequences with a fuzzy logic processing of the current responses is proposed to solve this problem. In [16], a PCI method based on the injection of controlled pulse currents is studied, but extra voltage sensors are needed to accomplish the measurement of the inverter terminal voltages. Compared with the HFSI based methods, the PSI based

The associate editor coordinating the review of this manuscript and approving it for publication was Jinquan Xu.

methods are easier to carry out without the complicated signal demodulation and magnetic polarity detection processes.

However, the conventional PVI based methods proposed in [13], [14] obtain the IRP with the virtual d-axis current (i_d^v) response of PMSM at standstill, and the information about the virtual q-axis current (i_q^v) response is not utilized. By analyzing the current response model of PMSM at standstill, it is found out that the variation of the virtual d-axis current is quite small if the angle of the injected VV is approach to the IRP. The real size relationship of i_d^v may fail to be computed correctly in the case where the sampling error of i_d^v is bigger than the variation of it caused by the change of the angle of the injected VV. Accordingly, the accuracy of the initial position detection of the conventional methods is greatly affected by the current sampling errors. In order to solve this problem, an improved PVI method based on both the virtual d and q-axis current responses is studied in this paper. According to the fact that the variation of i_q^v is relatively bigger than the variation of i_d^v with the angle of the injected VV approaching to the IRP, the information of i_q^v is utilized for the proposed method to reduce the estimation errors of IRP caused by the current sampling errors. The experimental results verify the effectiveness of the proposed method.

II. CURRENT RESPONSE MODEL OF PMSM AT STANDSTILL

For the PMSM at standstill, the voltage equations in the synchronously rotating reference frame can be described as

$$\begin{cases} u_d = R_s i_d + L_d \dfrac{di_d}{dt} \\ u_q = R_s i_q + L_q \dfrac{di_q}{dt} \end{cases} \tag{1}$$

where u_d, i_d, and L_d are the d-axis stator voltage, current and inductance, u_q, i_q, and L_q are the q-axis stator voltage, current and inductance, R_s is the stator resistance.

By discretizing (1) with the forward Euler method, the d and q-axis current responses can be obtained in (2), where the specific voltage vector is continuously applied to the motor for n control periods (T_c).

$$\begin{cases} i_d(n) = u_d \xi_d(n) \\ i_q(n) = u_q \xi_q(n) \end{cases} \tag{2}$$

where ξ_d(n) and ξ_q(n) satisfy

$$\begin{cases} \xi_d(n) = \dfrac{1}{R_s}\left[1 - \left(1 - \dfrac{R_s}{L_d} T_c\right)^n\right] \\ \xi_q(n) = \dfrac{1}{R_s}\left[1 - \left(1 - \dfrac{R_s}{L_q} T_c\right)^n\right] \end{cases} \tag{3}$$

$\Delta\xi$(n) is defined as (4) and it is positive because L_d is smaller than L_q.

$$\Delta\xi(n) = \xi_d(n) - \xi_q(n) \tag{4}$$

A virtual synchronously rotating reference frame (d^v-q^v) is defined in Figure. 1, where θ_V is the angle between the

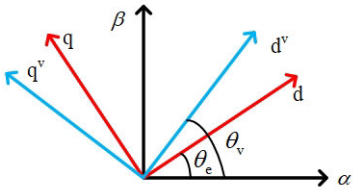

FIGURE 1. The virtual d-q frame.

d^v-axis and the α-axis and θ_e is the angle between the d-axis and the α-axis. The rotor flux is oriented to the permanent magnet flux of the rotor, and thus, θ_e is defined as the initial rotor position.

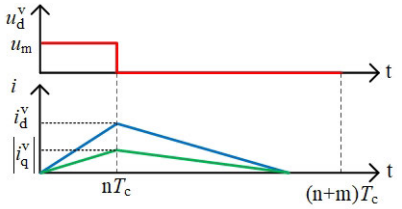

FIGURE 2. The virtual d and q-axis current response of PMSM at standstill.

If the voltage vector defined in (5) is continuously injected to the PMSM for n control periods, as shown in Figure. 2, the current in the d^v-q^v frame can be calculated by (6) where u_m is the amplitude of the injected voltage and it is positive. Then, all the gate signals of the inverter are turned off for m control periods to ensure each phase current become zero.

$$\begin{cases} u_d^v = u_m \\ u_q^v = 0 \end{cases} \tag{5}$$

$$\begin{cases} i_d^v(n) = u_m \xi_q(n) + u_m \Delta\xi(n) \cos^2(\theta_v - \theta_e) \\ i_q^v(n) = -\dfrac{1}{2} u_m \Delta\xi(n) \sin[2(\theta_v - \theta_e)] \end{cases} \tag{6}$$

III. THE CONVENTIONAL PVI BASED IRPEM

The variables u_m, $\Delta\xi_q$(n), and ξ(n) in (6) are all positive, and thus, i_d^v is maximal in the case where θ_V is equal to θ_e. The conventional IRPEM obtains the initial rotor position with the above principle using the virtual d-axis current response of PMSM at standstill.

The sequence diagram of injection voltage vectors for the conventional PVI based IRPEM is shown in Figure. 3. The amplitude of the whole 27 injection voltage vectors is identical. In Figure. 3 (a), 12 distinct voltage vectors are injected to the PMSM in numerical order, and the virtual d-axis current transformed from the measured three-phase currents (i_a, i_b, and i_c) is calculated as (7).

$$i_d^v = i_a \cos(\theta_V) + \frac{\sqrt{3}}{3}(i_b - i_c)\sin(\theta_V) \tag{7}$$

For the conventional method, the virtual d-axis current (i_d^v) corresponding to the injected voltage vector is calculated,

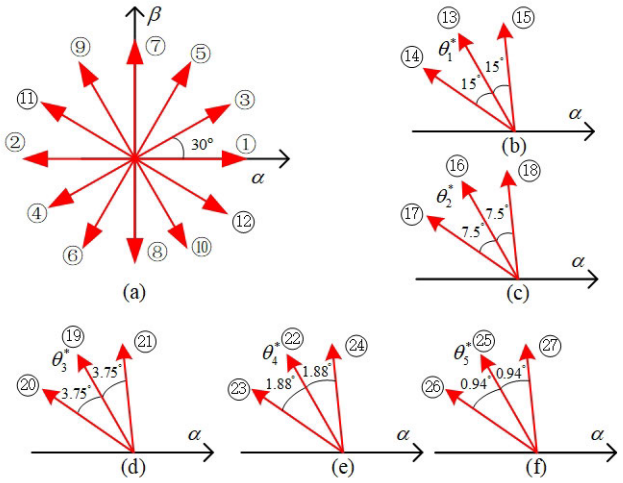

FIGURE 3. Sequence diagram of injection voltage vectors for the conventional PVI based IRPEM.

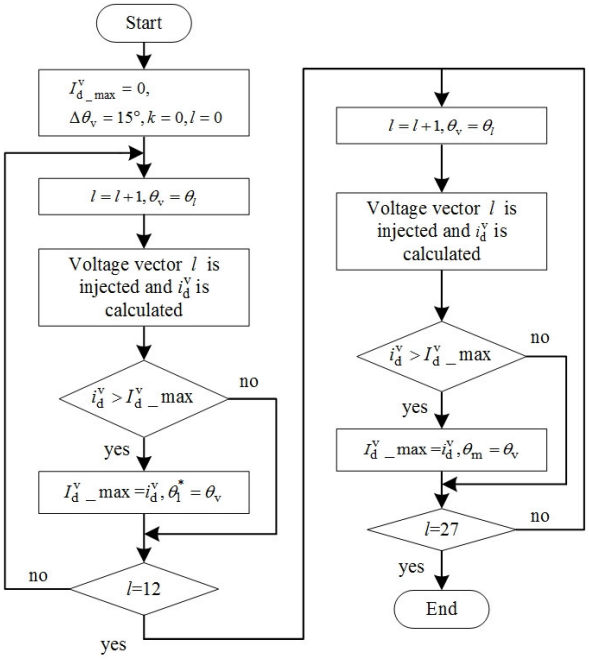

FIGURE 4. The flowchart of the conventional PVI based IRPEM.

and the voltage vector angle when the corresponding i^v_d is maximal is defined as θ^*_1. In Figure. 3 (b)-(f), $\theta^*_1 \sim \theta^*_5$ is the injected voltage vector angles corresponding to the maximum i^v_d in Fig. 3 (a)-(e), and $\Delta\theta$ is 15, 7.5, 3.75, 1.88, and 0.94 degrees, respectively. Three kinds of the voltage vectors of which the angles are θ^*_j, $\theta^*_j - \Delta\theta$, and $\theta^*_j + \Delta\theta$, as shown in Figure. 3 (b)-(f), are injected to PMSM, and the angle of the injected voltage vector that shows the maximum i^v_d equals the final estimated initial rotor position. The flowchart of the conventional PVI based IRPEM is shown in Figure. 4, where $I^v_{d\_max}$ represents the maximal value of i^v_d and the estimated IRP is defined as θ_m.

IV. THE IRPEM BASED ON VIRTUAL D AND Q-AXIS CURRENT RESPONSES

According to the above analysis, the conventional PVI based IRPEM method obtain the initial rotor position according the virtual d-axis current response of PMSM at standstill, and the information about the virtual q-axis current response is not utilized. In order to reduce the influence of sampling error on the accuracy of initial position detection, an improved IRPEM based on both the virtual d and q-axis current responses is studied.

A. PROBLEMS OF THE CONVENTIONAL PVI BASED IRPEM

To calculate i^v_d, the phase current is measured according to (8), where i^m_j, i_j, and Δi_j is the measured value, real value, and measurement error for the current of phase 'j' (j=a,b,c).

$$i^m_j = i_j + \Delta i_j \tag{8}$$

Δi_j depends on the accuracy of current sensor and zero drift of current sampling devices. Since the three-phase currents are measured by the same current sensors and analog-to-digital conversion circuits, it can be considered that the maximum measurement error of each phase current is consistent and it is defined as ΔI_m. Then, Δi_j ranges from -ΔI_m to ΔI_m.

According to (7) and (8), the calculate error of i^v_d (Δi^v_d) caused by the measurement error of phase currents is given in (9)

$$\Delta i^v_d = \Delta i_a \cos(\theta_V) + \sqrt{3}/3\,(\Delta i_b - \Delta i_c)\sin(\theta_V) \tag{9}$$

Theoretically, the expression of the maximum value of Δi^v_d ($\Delta I^v_{d\_m}$) is shown in (10), and then Δi^v_d ranges from $-\Delta I^v_{d\_m}$ to $\Delta I^v_{d\_m}$.

$$\Delta I^v_{d\_m} = \Delta I_m |\cos(\theta_V)| + 2\sqrt{3}/3\Delta I_m |\sin(\theta_V)| \tag{10}$$

It can be seen from (10) that $\Delta I^v_{d\_m}$ is related with θ_V and the curve of $\Delta I^v_{d\_m}$ with different θ_V is shown in Figure. 5.

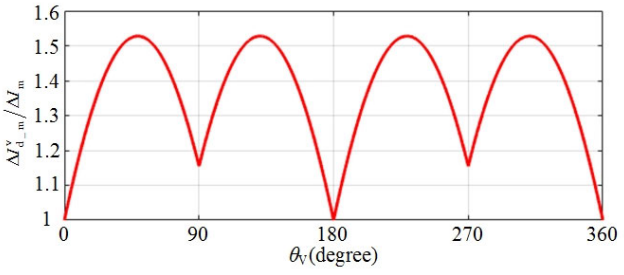

FIGURE 5. The curve of $\Delta I^v_{d\_m}$ with different θ_V.

The initial rotor position is estimated by the conventional PVI based IRPEM according to the size relationship of i^v_d with different injected voltage vector angles, thus, the accuracy of this method is influenced by the calculate error of i^v_d caused by the measurement error of phase currents.

According to (6), the derivative of $i^v_d(n)$ to θ_V is given in (11), and accordingly, it is 0 in the case where θ_V is

equal to θ_e.

$$\frac{di_d^v(n)}{d\theta_V} = -u_m \Delta\xi(n) \sin[2(\theta_V - \theta_e)] \tag{11}$$

In addition, the derivative of i_d^v to θ_V is small if the injected voltage vector angle is approach to IRP because the value of sine function in (11) is close to 0, and thus, the variation of i_d^v, as shown in Fig. 6, is relatively small in this case. In Fig. 6, L_d is 0.95mH, L_q is 2.05mH, R_s is 0.1 Ω, n is 10, and T_c is 100 μs. It can be seen that the difference of i_d^v between the case $\theta_V = \theta_e$ and the case θ_V-θ_e =5 degrees is only about 0.4A, which is about 0.4% of the maximum value of i_d^v.

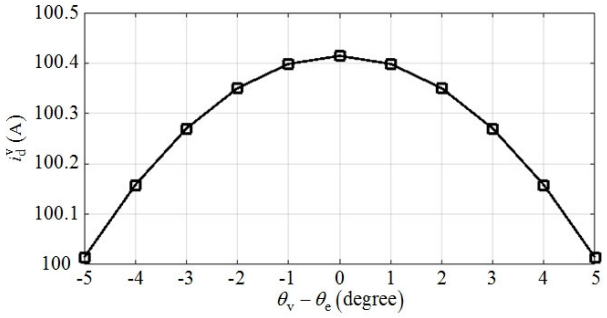

FIGURE 6. The curve of i_d^v in the case where θ_V is approach to θ_e.

As discussed above, the calculated i_d^v may not be identical to its actual value owing to the measurement error of phase currents. If Δi_d^v is bigger than variation of i_d^v caused by the change of θ_V, the real size relationship of i_d^v may fail to compute correctly. Accordingly, the accuracy of the conventional IRPEM method is greatly influenced by the sampling errors of phase currents because the variation of i_d^v is quite small in the case where θ_V is approach to θ_e.

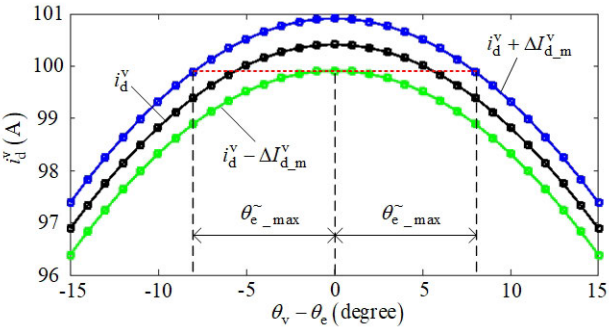

FIGURE 7. Analysis of the measurement error of the conventional PVI based IRPEM.

To further analyze, the actual, maximal, and minimal calculated value of i_d^v ($i_d^v + \Delta I_{d\_m}^v$, i_d^v-$\Delta I_{d\_m}^v$) are plotted in Figure. 7, where the IRP is set as 0, ΔI_m is 0.5A, and $\Delta I_{d\_m}^v$ is the same as ΔI_m according to Fig. 5. It can be seen that the calculated i_d^v in the case $\theta_V = \theta_e$ may become smaller than the calculated i_d^v with the θ_V satisfying (12), and the real size relationship of i_d^v with different θ_V may fail to compute correctly in the case as shown in (13) where the definition of $\tilde{\theta}_{e\_max}$ is shown in Figure. 7.

$$i_d^v(\theta_e) - i_d^v(\theta_v) \le 2\Delta I_{d\_m}^v \tag{12}$$

$$-\tilde{\theta}_{e\_max} \le \theta_v - \theta_e \le \tilde{\theta}_{e\_max} \tag{13}$$

Accordingly, the above analysis indicates that the measurement error of the conventional PVI based IRPEM may become big because the actual size relationship of i_d^v is hard to obtain in the case where θ_V is approach to θ_e.

B. PRINCIPLE OF THE PROPOSED PVI BASED IRPEM

Different from the conventional method that only utilizes the information about the virtual d-axis current for the voltage vector injected to PMSMs, the information about the virtual q-axis current is also utilized for the proposed method to reduce the estimation errors caused by the current sampling errors.

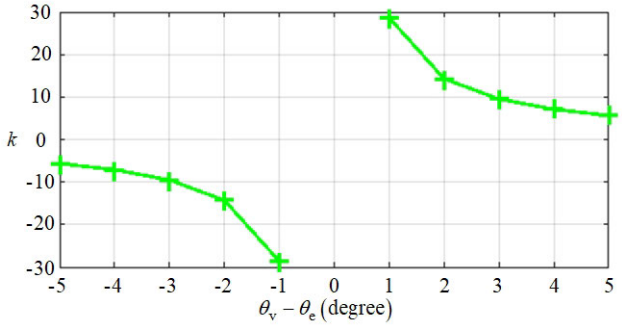

FIGURE 8. The curve of k.

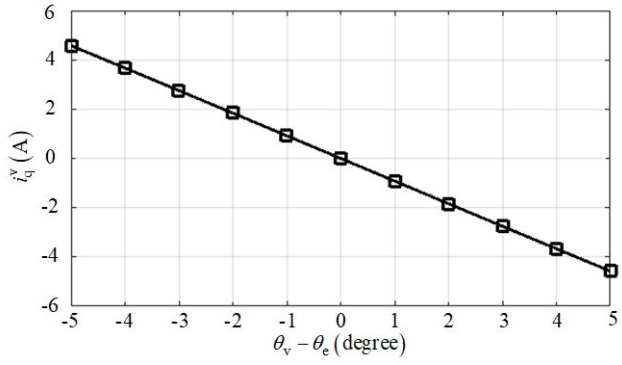

FIGURE 9. The curve of i_q^v in the case where θ_V is approach to θ_e.

According to (6), the derivative of i_q^v to θ_V is given in (14), and its absolute is maximal in the case where θ_V is equal to θ_e. The ratio of (14) to (11) is defined as k and its curve is shown in Figure. 8. It is indicated that the absolute value of the derivative of i_q^v to θ_V is greatly bigger than the derivative of i_d^v to θ_V when θ_V is approach to θ_e, i.e., the variation of i_q^v, as shown in Figure. 9, is relatively bigger than the variation of i_d^v as shown in Figure. 6. As an example, the difference of i_q^v between the case $\theta_V = \theta_e$ and the case $\theta_V - \theta_e = 5$ degrees

is about 4.58A, which is about 11.45 times of the variation of i_d^v in the same case.

$$\frac{di_q^v(n)}{d\theta_v} = -u_m \Delta\xi(n) \cos[2(\theta_v - \theta_e)] \quad (14)$$

Moreover, it can be seen from (6) that i_q^v is 0 if θ_V is equal to θ_e, and the absolute of i_q^v ($|i_q^v|$) becomes minimal in this case.

The block diagram of the proposed IRPEM is shown in Figure 10. The voltage vectors are sequentially injected to PMSM, and the information about the virtual d-axis and q-axis currents which are calculated by the measured three-phase currents. For the proposed method, the sequence diagram of injection voltage vectors is the same as shown in Figure. 3, but the measured IRP is updated according to the size relationship of $|i_q^v|$ in the process as shown in Figure. 3 (b)-(e), while θ_1^* is obtained according to the size relationship of i_d^v as the conventional method. The flowchart of the proposed IRPEM is given in Figure. 11 where $I_{q\_min}^v$ represents the minimal value of $|i_q^v|$.

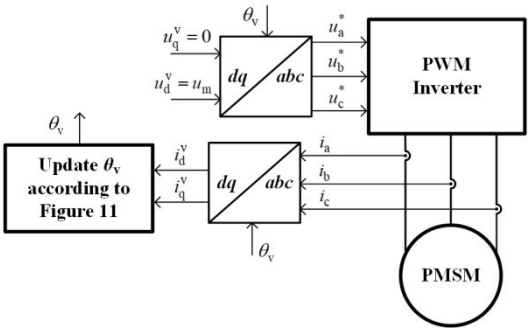

FIGURE 10. The block diagram of the proposed IRPEM.

For the proposed PSI based method, the magnitude and intervals of the injected VVs exert a major effect on estimation accuracy. As analyzed above, the magnitude of the responding current is positive correlation with the product of the magnitude and intervals of the injected VVs and it should be large enough to ensure that the current difference corresponding to two adjacent injected VVs is greater than the sampling error. With help of the locking device to keep the rotor of PMSM static, the maximum value of the response current should be close to the rated current to ensure the estimation accuracy. The proposed method of setting of the magnitude and intervals of the injected VVs is explained below. By adoption of the space vector pulse width modulation (SVPWM), the maximal value of u_m (u_{m_max}) is $0.575U_{dc}$, where U_{dc} is the dc-link voltage of inverter. Firstly, the amplitude of the injected VVs (u_m) is set from 75%-100% of u_{m_max} to decrease the execution time of the proposed method. After determining u_m, the NO. of injection intervals can be estimated by the maximal n that satisfies (15) where I_N is the rated current of PMSM.

$$\sqrt{\left(i_q^v(n)\right)^2 + \left(i_d^v(n)\right)^2} \le \sqrt{2} I_N \quad (15)$$

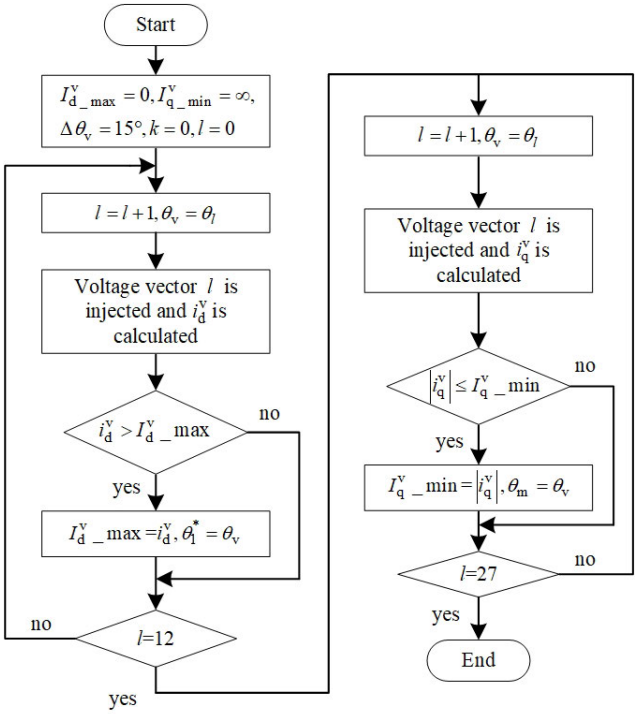

FIGURE 11. The flowchart of the proposed IRPEM.

C. COMPARISON ANALYSIS

To illustrate the advantage of the proposed method, comparison analysis is conducted in this part. For the proposed method, the virtual q-axis current transformed from the measured three-phase currents can be calculated as (16).

$$i_q^v = -i_a \sin(\theta_V) + \frac{\sqrt{3}}{3}(i_b - i_c)\cos(\theta_V) \quad (16)$$

According to (8) and (15), the calculate error of i_q^v (Δi_q^v) caused by the measurement error of phase currents is given in (17)

$$\Delta i_q^v = -\Delta i_a \sin(\theta_V) + \sqrt{3}/3\,(\Delta i_b - \Delta i_c)\cos(\theta_V) \quad (17)$$

Theoretically, the expression of the maximum value of Δi_q^v ($\Delta I_{q\_m}^v$) is shown in (18), and then Δi_q^v ranges from $-\Delta I_{q\_m}^v$ to $\Delta I_{q\_m}^v$.

$$\Delta I_{q\_m}^v = \Delta I_m |\sin(\theta_V)| + 2\sqrt{3}/3 \Delta I_m |\cos(\theta_V)| \quad (18)$$

It can be seen from (18) that $\Delta I_{q\_m}^v$ is related with θ_V and the curve of $\Delta I_{q\_m}^v$ with different θ_V is shown in Figure. 12. Compared with Figure. 5, it can be seen that the variation range of $\Delta I_{q\_m}^v$ is identical to $\Delta I_{d\_m}^v$.

Similar as the case of i_d^v, the real size relationship of i_q^v may fail to compute correctly if Δi_q^v is bigger than variation of i_q^v caused by the change of θ_V. Accordingly, the accuracy of the proposed IRPEM method is also affected by the sampling errors of phase currents. But fortunately, the variation of i_q^v is far bigger than i_d^v in the case where θ_V is approach to θ_e according to Figure. 8. The variation of i_q^v caused by

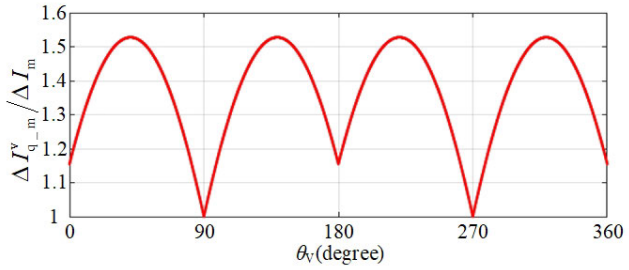

FIGURE 12. The curve of $\Delta i^{v}_{q\_m}$ with different θ_V.

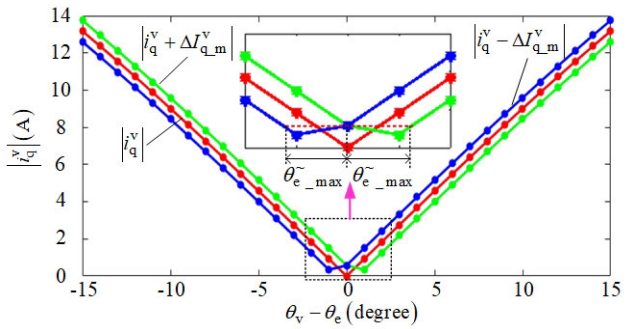

FIGURE 13. Analysis of the measurement error for the proposed PVI based IRPEM.

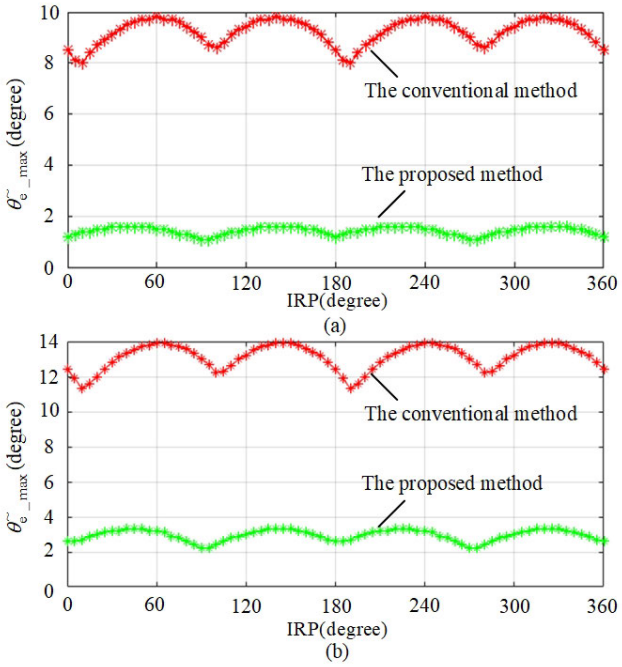

FIGURE 14. Comparison results of the maximal possible IRP estimation error. (a) ΔI_m is 0.5A. (b) ΔI_m is 1.0A.

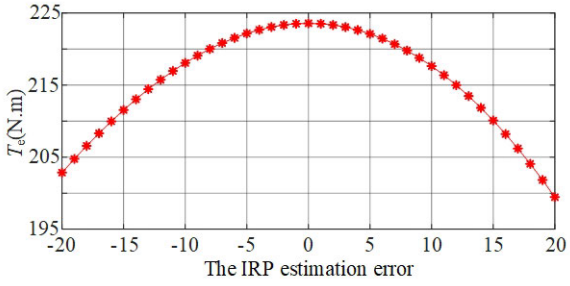

FIGURE 15. The curves of electromagnetic torque with various IRP estimation error.

the change of θ_V is bigger than Δi^{v}_q in most cases and the estimation error of IRP caused by measured error of current is greatly reduced. To further analyze, the actual, maximal, and minimal calculated value of i^{v}_q ($i^{v}_q + \Delta I^{v}_{q\_m}$, i^{v}_q-$\Delta I^{v}_{q\_m}$) are plotted in Figure. 13, where the IRP is set as 0, ΔI_m is 0.5A and $\Delta I^{v}_{d\_m}$ is about 0.577A according to Figure. 12.

It can be seen from the enlargement of Figure. 13 that the calculated $|i^{v}_q|$ in the case $\theta_V = \theta_e$ may become bigger than the calculated $|i^{v}_q|$ for the θ_V satisfying (19), and the real size relationship of $|i^{v}_q|$ with different θ_V may fail to compute correctly in the case as shown in (20) where the definition of $\theta^{\sim}_{e\_max}$ is shown in Figure. 13.

$$\left|i^{v}_q(\theta_v)\right| - \left|i^{v}_q(\theta_e)\right| \le 2\Delta I^{v}_{q\_m} \tag{19}$$

$$-\theta^{\sim}_{e\_max} \le \theta_v - \theta_e \le \theta^{\sim}_{e\_max} \tag{20}$$

In both Figure. 7 and Figure. 13, $\theta^{\sim}_{e\_max}$ represents the maximal possible IRP estimation error. According to the results shown in Figure. 7 and Figure. 13, the $\theta^{\sim}_{e\_max}$ for the conventional and proposed methods are about 8 degrees and 1 degree, respectively. Comparison results of $\theta^{\sim}_{e\_max}$ between the conventional and proposed methods are shown in Figure. 14. In Figure. 14 (a) and (b), ΔI_m is set as 0.5A and 1.0A, respectively. By comparing the results in Fig. 14 (a) and (b), the maximal possible IRP estimation error of the conventional and proposed methods increases with the increase of ΔI_m. In addition, $\theta^{\sim}_{e\_max}$ is changed with the IRP owing to $\Delta I^{v}_{d\_m}$ and $\Delta I^{v}_{q\_m}$ are not identical with different θ_V. It can be seen from Figure. 14 that the maximal possible IRP estimation error of the proposed method has been greatly reduced. Accordingly, the accuracy of the initial position detection can be improved with the proposed method.

The electromagnetic torque (T_e) of PMSMs can be calculated as (21) where P_n and ψ_f are the pole pairs and permanent magnet flux linkage of PMSMs.

$$T_e = 1.5P_n[\psi_f + (L_d - L_q)i_d]i_q \tag{21}$$

With the existence of IRP estimation error ($\theta^{\sim}_e$), the electromagnetic torque equation has changed as (22) owing to the angle difference between the actual d-axis and the used d-axis is $\theta^{\sim}_e$.

$$T_e = 1.5P_n\left[\psi_f + (L_d - L_q)\left(i^{v}_d\cos\left(\theta^{\sim}_e\right) - i^{v}_q\sin\left(\theta^{\sim}_e\right)\right)\right] * \left[i^{v}_q\cos\left(\theta^{\sim}_e\right) + i^{v}_d\sin\left(\theta^{\sim}_e\right)\right] \tag{22}$$

TABLE 1. Main parameters of the experimental prototype.

Paremeter	Value	Paremeter	Value
U_{dc}(V)	310	I_N(A)	100
u_m(V)	100	L_d(mH)	0.95
T_c(s)	1e-4	L_q(mH)	2.05
n	10	R_s(Ω)	0.1
m	90	P_n	4

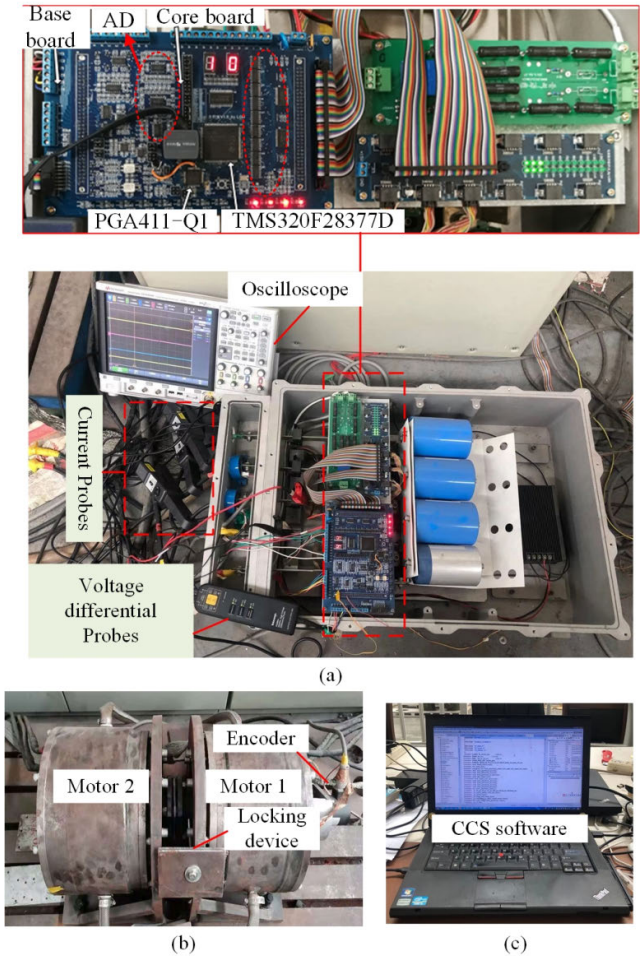

FIGURE 16. Photos of the experimental prototype.

When the maximum torque per ampere (MTPA) control is adopted, the relationship between i_d^v, i_q^v, and the amplitude of stator current (i_s) is given in (23)

$$\begin{cases} i_d^v = \dfrac{\psi_f}{4\left(L_q - L_d\right)} - \sqrt{\dfrac{\psi_f^2}{16\left(L_q - L_d\right)^2} + 0.5 i_s^2} \\ i_q^v = \sqrt{i_s^2 - \left(i_d^v\right)^2} \end{cases} \tag{23}$$

By combining (22) and (23), the electromagnetic torque with various $\theta_e^{\sim}$ can be calculated and the results are shown in Figure. 15 where the parameters of PMSM are shown in Table 1 and i_s is set as 144A. It is indicated by Figure. 15

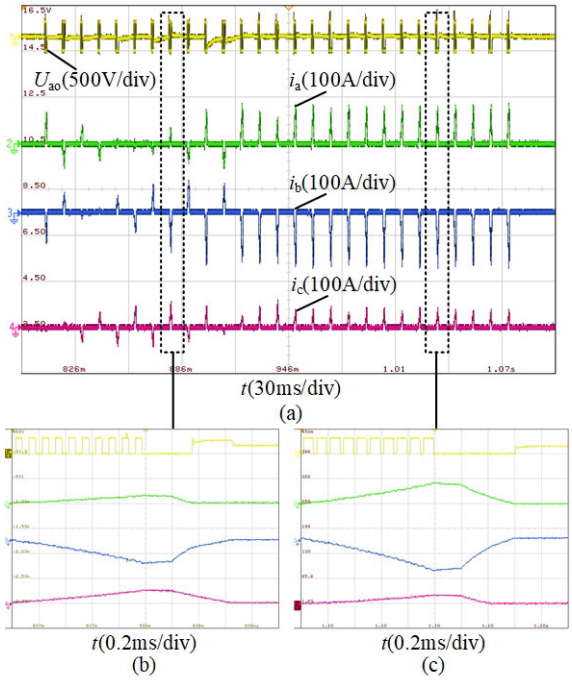

FIGURE 17. Voltage and current waveforms during the injection. (a) The whole process. (b) The enlargement waveforms of the 8th injection voltage vector. (c) The enlargement waveforms of the 23th injection voltage vector.

that the electromagnetic torque with the same stator current is decreased with the IRP estimation error increasing. Taking the IRP estimation errors shown in Figure. 7 and Figure. 13 as examples, the electromagnetic torque for the conventional and the proposed method with the IRP estimation error equal to $\theta_{e\_max}^{\sim}$ are 219.8 N.m and 223.5N.m. Accordingly, the electromagnetic torque increases with the same starting current with the proposed method.

V. EXPERIMENTAL RESULTS AND ANALYSIS

To verify the effectiveness of the proposed IRPEM, an experimental prototype as shown in Figure. 16 is established and the main parameters are listed in Table 1, where U_{dc}, T_c, I_N, and P_n represent the dc-link voltage, carrier frequency, rated current of PMSM, and pole pairs, respectively. The parameters L_d, L_q, R_s in Table 1 are measured by an impedance test instrument with a 200Hz, 10V sinusoidal voltage injection.

In the experimental prototype, a locking device as shown in Figure 16 (b) is adopted to keep the rotor of PMSM at standstill. In practical applications, the rotor of PMSM is often locked by a mechanical device such as a hydraulic station before it starts, so the algorithm in this paper can be applied to these occasions. The adopted 2L-inverter is shown in Figure. 16 (a) where three current probes are utilized to measure three-phase currents of PMSM. The virtual d and q-axe currents are calculated by the digital signal processor of which the type is TMS320F28377D. The calculated virtual d and q-axe currents are stored in arrays and can be

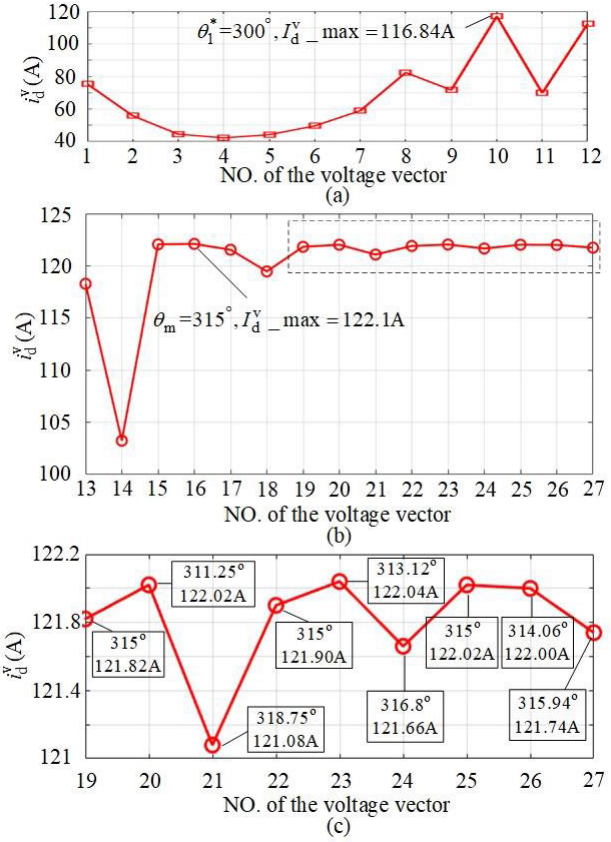

FIGURE 18. Estimation result for the conventional method when the actual angle is 310 degrees. (a) i_d^v in the process as shown in FIGURE 3. (a). (b) i_d^v in the process as shown in FIGURE 3. (b)-(f). (c) The enlargement of the contents in the dotted box of FIGURE 18. (b).

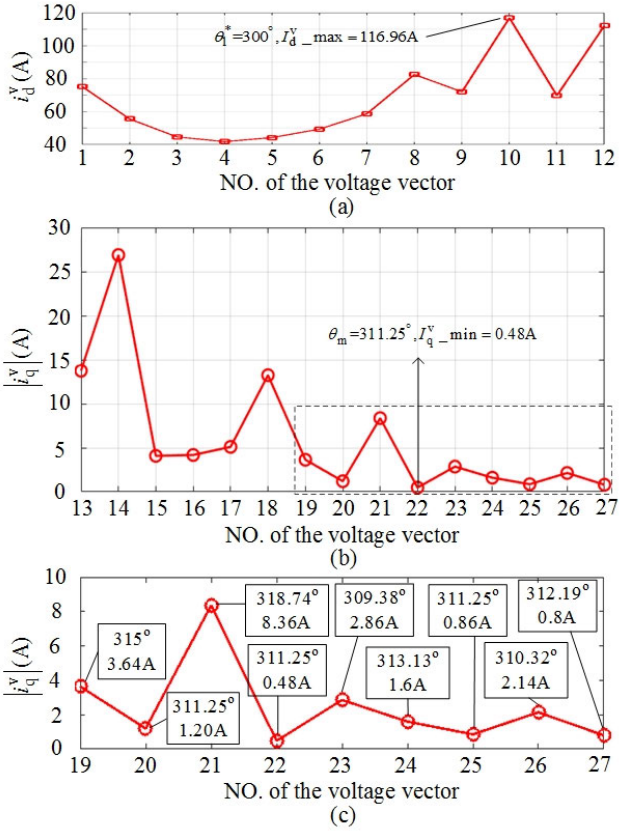

FIGURE 19. Estimation result for the conventional method when the actual angle is 310 degrees. (a) i_d^v in the process as shown in FIGURE 3. (a). (b) $|i_q^v|$ in the process as shown in FIGURE 3. (b)-(f). (c) The enlargement of the contents in the dotted box of FIGURE 19. (b).

observed by the software of code composed studio (CCS) as shown in Figure. 16 (c). Current transducers LF 210-S/SP1 produced by LEM electronics Co., Ltd are installed to measure the phase currents and the analogue inputs have been transformed into digital outputs through an AD module on the adopted digital signal processor (DSP) of which the type is TMS320F28377D. According to the datasheet of the current transducers and the observed noise of AD sampling, the maximal total measuring error of the phase current is estimated about 1.0 A.

As an example, the voltage and current waveforms during the injection process of the proposed method in the case that the actual angle is 310 degrees are shown in Figure. 17, where U_{ao} represents the voltage between phase 'a' and the negative terminal of the dc-link. As shown in the enlargement waveforms in Figure. 17 (b) and (c), the voltage vectors are injected continuously for 10 carrier periods (1ms), and the peak value of the virtual d-axis and q-axis currents are calculated according to the measured three-phase currents.

The estimation result for the conventional method when the actual angle is 310 degrees is shown in Figure. 18. The curve of i_d^v in the process shown in Figure. 3 (a) is given in Figure. 18 (a). The $I_{d\_max}^v$ in this process is 116.84A and θ_1^* is 300 degrees. The curve of i_d^v in the process shown in Fig. 3 (b)-(f) is given in Figure. 18 (b). From the enlargement of the result for the injected voltage vector 19-27 as shown in Fig. 18 (c), it can be seen that the variation of i_d^v in this case is relatively small. The largest difference of i_d^v in the enlargement is only 0.96A, which is smaller than the maximal total measuring error of the phase current. The measured and calculating error of i_d^v may be bigger than the variation of i_d^v caused by the change of θ_V, and the real size relationship of i_d^v may fail to compute correctly. Accordingly, the accuracy of the conventional method is greatly influenced by the precise of the measurement and calculation of i_d^v. The final estimated IRP with the conventional method is 315 degrees, and the estimated error is 5 degrees.

The estimation result for the proposed method when the actual angle is 310 degrees is shown in Figure. 19. The curve of i_d^v in the process shown in Figure. 3 (a) is given in Figure. 19 (a). The $I_{d\_max}^v$ in this process is 116.96A and θ_1^* is 300 degrees. The curve of $|i_q^v|$ in the process shown in Figure. 3 (b)-(f) is given in Figure. 19 (b). From the

enlargement of the result for the injected voltage vector 19-27 as shown in Figure. 19 (c), it can be seen that the largest difference of $|i_q^v|$ in the enlargement is 7.88A, which is about 820.8% of the largest difference of i_d^v as shown in Figure. 18 (c). Accordingly, the influence of sampling error on the proposed method is greatly reduced compared with the conventional one. The final estimated IRP with the proposed method is 311.25 degrees, and the estimated error is 1.25 degrees, which has been reduced by 74.8% compared with the conventional method.

To analyze the estimation error, the IRP detection experiments were carried out for 20 times for each specific IRP with both the conventional and the proposed methods, and the average estimation errors corresponding to different IRPs were collectively given in Figure. 20. The result indicates that the estimation errors for the proposed method have been reduced by 37.5%-84.0% compared with the conventional one.

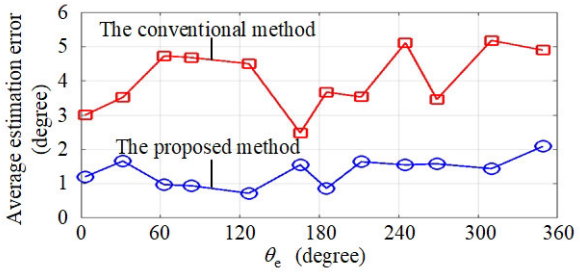

FIGURE 20. Estimation error analysis result.

VI. CONCLUSION

To increase estimation accuracy of the IRP for PMSMs, an improved PVI method based on both the virtual d and q-axis current responses has been studied in this paper. The proposed method is based on the principle that the virtual d-axis current for the VV applied to PMSMs increases and the absolute of the virtual q-axis current decreases as the injected VV approaches to the north pole of the rotor. The experimental results indicate that the estimation errors for the proposed method have been reduced by 37.5%-84.0% compared with the conventional method.

REFERENCES

[1] H. Wang, K. Lu, D. Wang, and F. Blaabjerg, "Online identification of intrinsic load current dependent position estimation error for sensorless PMSM drives," *IEEE Access*, vol. 8, pp. 163186–163196, 2020.

[2] S. Chen, X. Wu, J. Chen, G. Tan, and Y. Wang, "Second-order lead compensator-based quadrature PLL for sensorless interior permanent magnet synchronous motor control," *IET Power Electron.*, vol. 13, no. 3, pp. 568–575, Feb. 2020.

[3] J. Xing, Z. Qin, C. Lin, and X. Jiang, "Research on startup process for sensorless control of PMSMs based on I-F method combined with an adaptive compensator," *IEEE Access*, vol. 8, pp. 70812–70821, 2020.

[4] M. Noman, G. Li, K. Wang, and B. Han, "Electrical control strategy for an ocean energy conversion system," *Protection Control Mod. Power Syst.*, vol. 6, no. 1, p. 12, Dec. 2021.

[5] B. Shuang and Z.-Q. Zhu, "A novel sensorless initial position estimation and startup method," *IEEE Trans. Ind. Electron.*, vol. 68, no. 4, pp. 2964–2975, Apr. 2021, doi: 10.1109/TIE.2020.2977551.

[6] X. Zhang, H. Li, S. Yang, and M. Ma, "Improved initial rotor position estimation for PMSM drives based on HF pulsating voltage signal injection," *IEEE Trans. Ind. Electron.*, vol. 65, no. 6, pp. 4702–4713, Jun. 2018.

[7] G. Bi, G. Wang, G. Zhang, N. Zhao, and D. Xu, "Low-noise initial position detection method for sensorless permanent magnet synchronous motor drives," *IEEE Trans. Power Electron.*, vol. 35, no. 12, pp. 13333–13344, Dec. 2020.

[8] X. Wu, Y. Feng, X. Liu, S. Huang, X. Yuan, J. Gao, and J. Zheng, "Initial rotor position detection for sensorless interior PMSM with square-wave voltage injection," *IEEE Trans. Magn.*, vol. 53, no. 11, pp. 1–4, Nov. 2017.

[9] X. Jin, R. Ni, W. Chen, F. Blaabjerg, and D. Xu, "High-frequency voltage-injection methods and observer design for initial position detection of permanent magnet synchronous machines," *IEEE Trans. Power Electron.*, vol. 33, no. 9, pp. 7971–7979, Sep. 2018.

[10] Y. Zhang, Z. Yin, J. Liu, R. Zhang, and X. Sun, "IPMSM sensorless control using high-frequency voltage injection method with random switching frequency for audible noise improvement," *IEEE Trans. Ind. Electron.*, vol. 67, no. 7, pp. 6019–6030, Jul. 2020.

[11] X. Wu, S. Huang, X. Liu, K. Lu, J. Gao, and J. Zheng, "Design of position estimation strategy of sensorless interior PMSM at standstill using minimum voltage vector injection method," *IEEE Trans. Magn.*, vol. 53, no. 11, pp. 1–4, Nov. 2017.

[12] B. Han, Y. Shi, X. Song, K. Hong, and K. Mao, "Initial rotor position detection method of SPMSM based on new high frequency voltage injection method," *IEEE Trans. Power Electron.*, vol. 34, no. 4, pp. 3553–3562, Apr. 2019.

[13] K. Tanaka, R. Moriyama, and I. Miki, "Initial rotor position estimation of interior permanent magnet synchronous motor using optimal voltage vector," *IEEJ Trans. Ind. Appl.*, vol. 124, no. 1, pp. 101–107, 2004.

[14] S. Nakashima, Y. Inagaki, and I. Miki, "Sensorless initial rotor position estimation of surface permanent-magnet synchronous motor," *IEEE Trans. Ind. Appl.*, vol. 36, no. 6, pp. 1598–1603, Nov. 2000.

[15] M. Tursini, R. Petrella, and F. Parasiliti, "Initial rotor position estimation method for PM motors," *IEEE Trans. Ind. Appl.*, vol. 39, no. 6, pp. 1630–1640, Nov. 2003.

[16] F. J. Anayi and M. M. A. Al Ibraheemi, "Estimation of rotor position for permanent magnet synchronous motor at standstill using sensorless voltage control scheme," *IEEE/ASME Trans. Mechatronics*, vol. 25, no. 3, pp. 1612–1621, Jun. 2020.

XIANG WU (Member, IEEE) was born in Jiangsu, China, in 1990. He received the B.S. and Ph.D. degrees in electrical engineering and automation from China University of Mining and Technology, Xuzhou, China, in 2013 and 2019, respectively. He is currently a Lecturer of power electronics and electrical drives with the School of Electrical and Power Engineering, China University of Mining and Technology. His research interests include power electronics, modern control theory, battery management systems, and motor.

ZEHAO LV was born in Zhejiang, China, in 1997. He received the B.S. degree in electrical engineering from Fuzhou University, Fuzhou, China, in 2019. He is currently pursuing the M.S. degree in power electronics and electrical drives with the School of Electrical and Power Engineering, China University of Mining and Technology, Xuzhou, China.

His current research interests include permanent magnet synchronous motor drives and model predictive control.

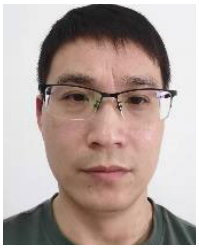

ZANG LING was born in Anhui, China, in 1982. He received the M.S. degree from the School of Information and Electrical Engineering, China University of Mining and Technology, Xuzhou, China, in 2009, where he is currently pursuing the Ph.D. degree in power electronics and electrical drives with the School of Electrical and Power Engineering. His current research interests include power electronic converters and the application of power electronics in renewable energy systems and motor control.

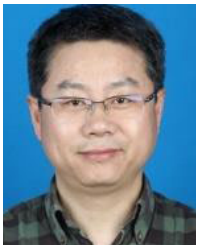

XIAO ZHANG was born in Baoji, China, in 1974. He received the M.S. and Ph.D. degrees from the School of Information and Electrical Engineering, China University of Mining and Technology, Xuzhou, China, in 2003 and 2012, respectively. In 1997, he joined as a Teaching Assistant at China University of Mining and Technology, where he has been an Associate Professor, since 2009. From October 2013 to October 2014, he was a Visiting Professor with The Ohio State University, Columbus, OH, USA. His current research interests include power electronic converters, reactive power control, harmonics, power quality compensation systems, and the application of power electronics in renewable energy systems and motor control.

GUOJUN TAN (Member, IEEE) was born in Zunyi, Guizhou, China, in 1962. He received the Ph.D. degree in motor driver and its automation from China University of Mining and Technology, Xuzhou, China, in 1992.

Since 2000, he has been a Professor with the School of Information and Electrical Engineering, China University of Mining and Technology. Since 2003, he has been the Chief Professor with the National Key Discipline on Power Electronics and Motor Driver, School of Information and Electrical Engineering. His main research interests include electrical drive, intelligent algorithm, and system optimization.